PROCESS-BASED MAPPING USING SPECTRAL INDICATORS IN AN IMAGE TEMPLATE MATCHING APPROACH

F.J.A. van Ruitenbeek, H.M.A. van der Werff & F.D. van der Meer

International Institute for Geo-information Science and Earth Observation (ITC),
Department of Earth Systems Analysis,
POBox 6, 7500 AA Enschede, The Netherlands,
{vanruitenbeek,vdwerff,vdmeer}@itc.nl

KEY WORDS: Supervised, edge detection, hyperspectral, image processing, hydrothermal alteration, boundary, white mica.

ABSTRACT

In geologic imaging spectroscopy studies, typical end products are often mineral maps. These maps are usually ambiguous and form a limited method of representing geological information that is potentially contained in spectroscopic images. This situation can be improved by mapping the spatial configuration of the effects of geological processes instead of the solely individual minerals in a non-spatial context. This so-called process-based mapping opens the way for a truly contextual mapping approach since the spectrally detectable expressions of processes occur in specific spatial arrangements. The contextual approach will solve the ambiguity problem occurring in mineral maps and will facilitate targeting of geologic processes. End products of this approach are not mineral maps but a map of the geological process.

A typical geologic process that is suitable for mapping using airborne imaging spectroscopy is submarine hydrothermal fluid circulation. Fluid pathways in fossil hydrothermal systems mark the start, the course, and the end fluid circulation from sites of recharge to sites of discharge. Boundaries between alteration facies along fluid pathways are zones where physico-chemical conditions change and these are required for reconstruction of the affects of hydrothermal processes and fluid pathways. In this paper, we demonstrate that we are able to map the various boundary zones in a fossil hydrothermal system using HyMap hyperspectral imagery in a contextual image processing approach using the RTM algorithm. The boundary zones between specific neighboring alteration assemblages were identified from spectral indicator images derived form airborne HyMap data. The supervised detection of boundary zones using this method is unbiased and selective to user-defined settings. Results in this study are useful for studies on hydrothermal systems and in particular in the search for early life on earth and other planets and in the exploration for hydrothermally formed mineralizations.

1 INTRODUCTION

Detection of boundaries by edge operators is widely applied to remotely sensed imagery, ranging from grey-level and multispectral to hyperspectral imagery (Bakker and Schmidt, 2002). The high spectral information content in hyperspectral images allows a detailed description of boundaries and favours the use of a supervised boundary detection algorithm. A boundary in an image is defined by the existence of at least two spectrally or texturally contrasting areas, and can as such be described by an image template. This paper presents the results of supervised boundary detection in a hyperspectral scene by using the "rotation-variant template matching" (RTM) algorithm (van der Werff *et al.*, 2005).

Template matching is a pattern recognition technique that is widely used for detection of objects in grey-level images (Tsai and Chiang, 2002). In the past, it has been applied for machine vision such as optical character recognition, face detection, object detection and defect detection (Tsai and Yang, 2005). In our paper, a template is a 1 dimensional image consisting of approx. 10 pixels. This template image contains information of a boundary between two spectrally contrasting regions. The template is moved over the image like a moving kernel. At every position, the template is rotated and a statistical fit is calculated for every pose (figure 1).

Rotation invariance is a desirable and often studied feature in template matching (Ullah and Kaneko, 2004), as conventional spatial cross-correlation algorithms cannot be applied when an object can be rotated (Choi and Kim, 2002). However, the variance in spectral fit of the template obtained by fitting at different orientations contains pertinent information that can be used for interpretation of the spectral signature of an object. The RTM algorithm has consequently been designed to be rotational variant (van der Werff *et al.*, 2005).

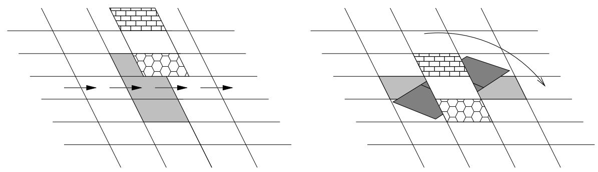

(a) a template moves... (b) ...and rotates

Figure 1: A template is matched by (a) moving it over an image and (b) changing the template orientation at every position by 45° increments up to a total of eight orientations.

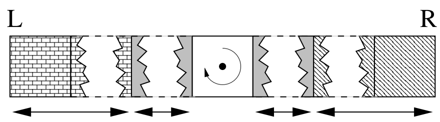

Figure 2: The template consists of 5 components, the centre pixel and, on each side, a margin of 0 or more pixels and 1 or more pixels with a user-defined reference value.

The RTM algorithm is first applied to synthetic data to clarify and evaluate the algorithm output. Next, the algorithm is applied to a hyperspectral image that covers an Archaic hydrothermal alteration system in the Pilbara, Australia, with the aim of detecting boundaries between specific mineral assemblages in this system that resulted from hydrothermal alteration processes.

2 THE RTM ALGORITHM

The RTM algorithm was described by van der Werff *et al.* (2005) and applied for the detection of boundaries between several mineral assemblages in a hydrothermal alteration systems. The templates were composed of shortwave infrared (SWIR) spectra and

4	5	4	5	4	5	5	5	5	5	5	5	2	5	2	5	2	5	2	5
5	6	5	6	5	5	5	5	5	5	5	5	5	8	5	8	5	8	5	8
4	5	4	5	4	5	5	5	5	5	5	5	2	5	2	5	2	5	2	5
5	6	5	6	5	5	5	5	5	5	5	5	5	8	5	8	5	8	5	8
4	5	4	5	4	5	5	5	5	5	5	5	2	5	2	5	2	5	2	5
5	6	5	6	5	5	5	5	5	5	5	5	5	8	5	8	5	8	5	8
4	5	4	5	4	5	5	5	5	5	5	5	5	5	5	5	5	5	5	5
5	6	5	6	5	5	5	5	5	5	5	5	5	5	5	5	5	5	5	5
4	5	4	5	4	5	5	5	5	5	5	5	5	5	5	5	5	5	5	5
5	6	5	6	5	5	5	5	5	5	5	5	5	5	5	5	5	5	5	5
8	8	8	8	8	8	8	8	8	8	5	5	5	5	5	5	5	5	5	5
8	8	8	8	8	8	8	8	8	8	5	5	5	5	5	5	5	5	5	5
8	8	8	8	8	8	8	8	8	8	5	5	5	5	5	5	5	5	5	5
8	8	8	8	8	8	8	8	8	8	5	5	5	5	5	5	5	5	5	5
8	8	8	8	8	8	8	8	8	8	5	5	5	5	5	5	5	5	5	5
8	8	8	8	8	8	8	8	8	8	2	2	2	2	2	2	2	2	2	2
8	8	8	8	8	8	8	8	8	8	2	2	2	2	2	2	2	2	2	2
8	8	8	8	8	8	8	8	8	8	2	2	2	2	2	2	2	2	2	2
8	8	8	8	8	8	8	8	8	8	2	2	2	2	2	2	2	2	2	2
8	8	8	8	8	8	8	8	8	8	2	2	2	2	2	2	2	2	2	2

(a) artificial image

N	N	N	N	N	N	N	N	N	N	N	N	N	N	N	N	N	N	N	N
N	N	N	N	N	N	N	N	N	N	N	N	N	N	N	N	N	N	N	N
N	N	N	N	N	N	N	N	N	N	N	N	N	N	N	N	N	N	N	N
N	N	N	N	N	N	N	N	N	N	N	N	N	N	N	N	N	N	N	N
N	N	N	N	N	N	N	N	N	N	N	N	N	N	N	N	N	N	N	N
N	N	N	N	N	N	N	N	N	N	N	N	N	N	N	N	N	N	N	N
N	N	N	N	N	N	N	N	N	N	N	N	N	N	N	N	N	N	N	N
N	N	N	N	N	N	N	N	N	N	N	N	N	N	N	N	N	N	N	N
N	N	N	N	N	N	N	N	N	N	N	N	N	N	N	N	N	N	N	N
N	N	1	N	1	1	1	1	1	1	1	N	N	N	N	N	N	N	N	N
N	N	N	1	1	1	1	1	1	1	1	N	N	N	N	N	N	N	N	N
N	N	N	N	N	N	N	N	N	1	1	N	N	N	N	N	N	N	N	N
N	N	N	N	N	N	N	N	N	1	1	N	N	N	N	N	N	N	N	N
N	N	N	N	N	N	N	N	N	1	1	N	N	N	N	N	N	N	N	N
N	N	N	N	N	N	N	N	N	1	1	N	N	N	N	N	N	N	N	N
N	N	N	N	N	N	N	N	N	1	1	N	N	N	N	N	N	N	N	N
N	N	N	N	N	N	N	N	N	N	N	N	N	N	N	N	N	N	N	N
N	N	N	N	N	N	N	N	N	N	N	N	N	N	N	N	N	N	N	N
N	N	N	N	N	N	N	N	N	N	N	N	N	N	N	N	N	N	N	N
N	N	N	N	N	N	N	N	N	N	N	N	N	N	N	N	N	N	N	N

(b) template match

NaN	NaN	NaN	NaN	NaN	NaN	NaN	NaN	NaN	NaN	NaN	NaN	NaN	NaN	NaN	NaN	NaN	NaN	NaN	NaN
NaN	NaN	NaN	NaN	NaN	NaN	NaN	NaN	NaN	NaN	NaN	NaN	NaN	NaN	NaN	NaN	NaN	NaN	NaN	NaN
NaN	NaN	NaN	NaN	NaN	NaN	NaN	NaN	NaN	NaN	NaN	NaN	NaN	NaN	NaN	NaN	NaN	NaN	NaN	NaN
NaN	NaN	NaN	NaN	NaN	NaN	NaN	NaN	NaN	NaN	NaN	NaN	NaN	NaN	NaN	NaN	NaN	NaN	NaN	NaN
NaN	NaN	NaN	NaN	NaN	NaN	NaN	NaN	NaN	NaN	NaN	NaN	NaN	NaN	NaN	NaN	NaN	NaN	NaN	NaN
NaN	NaN	NaN	NaN	NaN	NaN	NaN	NaN	NaN	NaN	NaN	NaN	NaN	NaN	NaN	NaN	NaN	NaN	NaN	NaN
NaN	NaN	NaN	NaN	NaN	NaN	NaN	NaN	NaN	NaN	NaN	NaN	NaN	NaN	NaN	NaN	NaN	NaN	NaN	NaN
NaN	NaN	NaN	NaN	NaN	NaN	NaN	NaN	NaN	NaN	NaN	NaN	NaN	NaN	NaN	NaN	NaN	NaN	NaN	NaN
NaN	NaN	NaN	NaN	NaN	NaN	NaN	NaN	NaN	NaN	NaN	NaN	NaN	NaN	NaN	NaN	NaN	NaN	NaN	NaN
NaN	NaN	90	NaN	90	116	90	90	116	116	135	NaN	NaN	NaN	NaN	NaN	NaN	NaN	NaN	NaN
NaN	NaN	NaN	90	135	90	116	90	116	135	153	NaN	NaN	NaN	NaN	NaN	NaN	NaN	NaN	NaN
NaN	NaN	NaN	NaN	NaN	NaN	NaN	NaN	NaN	153	153	NaN	NaN	NaN	NaN	NaN	NaN	NaN	NaN	NaN
NaN	NaN	NaN	NaN	NaN	NaN	NaN	NaN	NaN	180	180	NaN	NaN	NaN	NaN	NaN	NaN	NaN	NaN	NaN
NaN	NaN	NaN	NaN	NaN	NaN	NaN	NaN	NaN	153	153	NaN	NaN	NaN	NaN	NaN	NaN	NaN	NaN	NaN
NaN	NaN	NaN	NaN	NaN	NaN	NaN	NaN	NaN	153	153	NaN	NaN	NaN	NaN	NaN	NaN	NaN	NaN	NaN
NaN	NaN	NaN	NaN	NaN	NaN	NaN	NaN	NaN	135	135	NaN	NaN	NaN	NaN	NaN	NaN	NaN	NaN	NaN
NaN	NaN	NaN	NaN	NaN	NaN	NaN	NaN	NaN	NaN	NaN	NaN	NaN	NaN	NaN	NaN	NaN	NaN	NaN	NaN
NaN	NaN	NaN	NaN	NaN	NaN	NaN	NaN	NaN	NaN	NaN	NaN	NaN	NaN	NaN	NaN	NaN	NaN	NaN	NaN
NaN	NaN	NaN	NaN	NaN	NaN	NaN	NaN	NaN	NaN	NaN	NaN	NaN	NaN	NaN	NaN	NaN	NaN	NaN	NaN
NaN	NaN	NaN	NaN	NaN	NaN	NaN	NaN	NaN	NaN	NaN	NaN	NaN	NaN	NaN	NaN	NaN	NaN	NaN	NaN

(c) optimal orientation

Figure 3: The result of RTM on an artificial image. Careful examination learns that the algorithm only identifies the boundary pixels as defined in the template.

matched to an image, using the spectral angle (Kruse *et al.*, 1993) as a measure for spectral fit. In this paper, the RTM algorithm matches a user-defined template to a series of grey-scale images, each representing a product derived from a hyperspectral image.

A template is designed as a 1 dimensional image and consists of five components (figure 2). The centre pixel is the centre of rotation and is also used to store the template matching information for each position. The value of the centre pixel itself is ignored. This allows a crisp boundary, which theoretically would fall in between two image pixels, to be indicated by a double-pixel line centered around the theoretical position of the boundary. Each side of a template consists of pixels with a reference value and a margin. The margin consists of zero or more pixels and can be used for the detection of fuzzy boundaries. The reference values are defined in one or more pixels and are defined as a range in which an image value has to fall in order to be considered a positive match. A higher number of reference pixels requires more image pixels to fit in the user-defined range. This results in a more sensitive (non-binary) boundary detection at the cost of computational speed.

The RTM algorithm moves the template over an image, and at each position, the template is rotated in 45° increments to find the optimal fit and its orientation. For each pose of the template, the fit of the left and right side of the template is calculated as the mean of the number of reference pixels. In case both sides of the template have a positive match, the fit of the entire template is calculated as the mean of the left and right side fit. When all eight template orientations have been evaluated, the highest fit is selected and, with its orientation, written to the output image. In case more than one orientations result in an optimal fit, the mean angle of these optimal orientations is calculated. An angle between 1 and 360 indicates a preferred orientation, while an angle of 0 indicates that there was no preferred orientation found. A value of -1 is set as preferred orientation when the user-defined settings of the template are equal for the left and right side. The resulting image shows, for each pixel, the optimal fit of the template and the orientation at which this fit has been found.

In the last step, two of the template matching output images are combined by finding the pixels that are found to have a positive template match and, in addition, an equal orientation. The second criterium is waved in case either of the input images has no preferred orientation indicated by an angle of zero or, in case a symmetric template was applied, -1.

3 ARTIFICIAL IMAGERY

The RTM algorithm was first tested on an artificial image (Fig. 3(a)). A template of three pixels (value left (8), center pixel, value right (5)) was designed for detection of only those boundaries where five-values neighbor eight-values. The template matching result obtained on the artifical image is displayed in Fig. 3(b). Pixels that were positively identified as boundary pixels are indicated by one-values. The matching angle, i.e. the rotation angle of the template when it matched, is displayed in Fig. 3(c). Careful examination of the results shows the method is successful and that the RTM algorithm only identifies those boundary pixels that strictly match the template and that it is not confused by other boundaries.

4 HYMAP IMAGERY

4.1 Geological setting

The RTM algorithm was applied to Hymap (Cocks *et al.*, 1998) airborne hyperspectral data. The area that was selected was the hydrothermally altered footwall of the Kangaroo Caves massif sulfide deposit in the Pilbara, Western Australia (Fig. 5A). The area, which is part of a greenstone sequence, was strongly affected by hydrothermal processes in the Archean. The hydrothermal processes modified mineralogical compositions and variations in mineralogy reflected changing physico-chemical conditions (Brauhart *et al.*, 1998). Studying boundaries between mineral assemblages, or alteration facies, offers opportunities for reconstructing hydrothermal processes. Cudahy *et al.* (1999) and Van Ruitenbeek *et al.* (2005) demonstrated that various alteration facies can be identified using spectrally derived indices, presence of white micas and their Al-content. These indices were mapped from Hymap imagery using band ratios and multiple regression. The procedure is described in Van Ruitenbeek *et al.* (2006) and involves prediction of the presence of white mica using:

$$\mathtt{P}_{wm} = \frac{1}{1 + e^{\left(97.31 - 71.89 * \left(\frac{L_{2168nm}}{L_{2185nm}}\right) - 45.87 * \left(\frac{L_{2005nm}}{L_{2079nm}}\right)\right)}} \quad (1)$$

where L_u equals the radiance value of the airborne spectral band with centre wavelength u. The resulting white mica probability image calculated for the test area is shown in Fig. 5C. The wavelength position of the reflectance minimum of the main absorption feature of white micas, which is a measure for their Al-content, was estimated using:

$$\lambda_a = 2267.78 - 146.17 * \left(\frac{L_{2220nm}}{L_{2202nm}}\right) + 91.00 * \left(\frac{L_{2237nm}}{L_{2220nm}}\right) \quad (2)$$

where L_i equals the radiance value of airborne spectral band with center wavelength i. The resulting absorption wavelength image is displayed in Fig. 5D. The white mica probability and the absorption wavelength images were used as input for the RTM algorithm. The design of the template that was matched to these images is described in the following section.

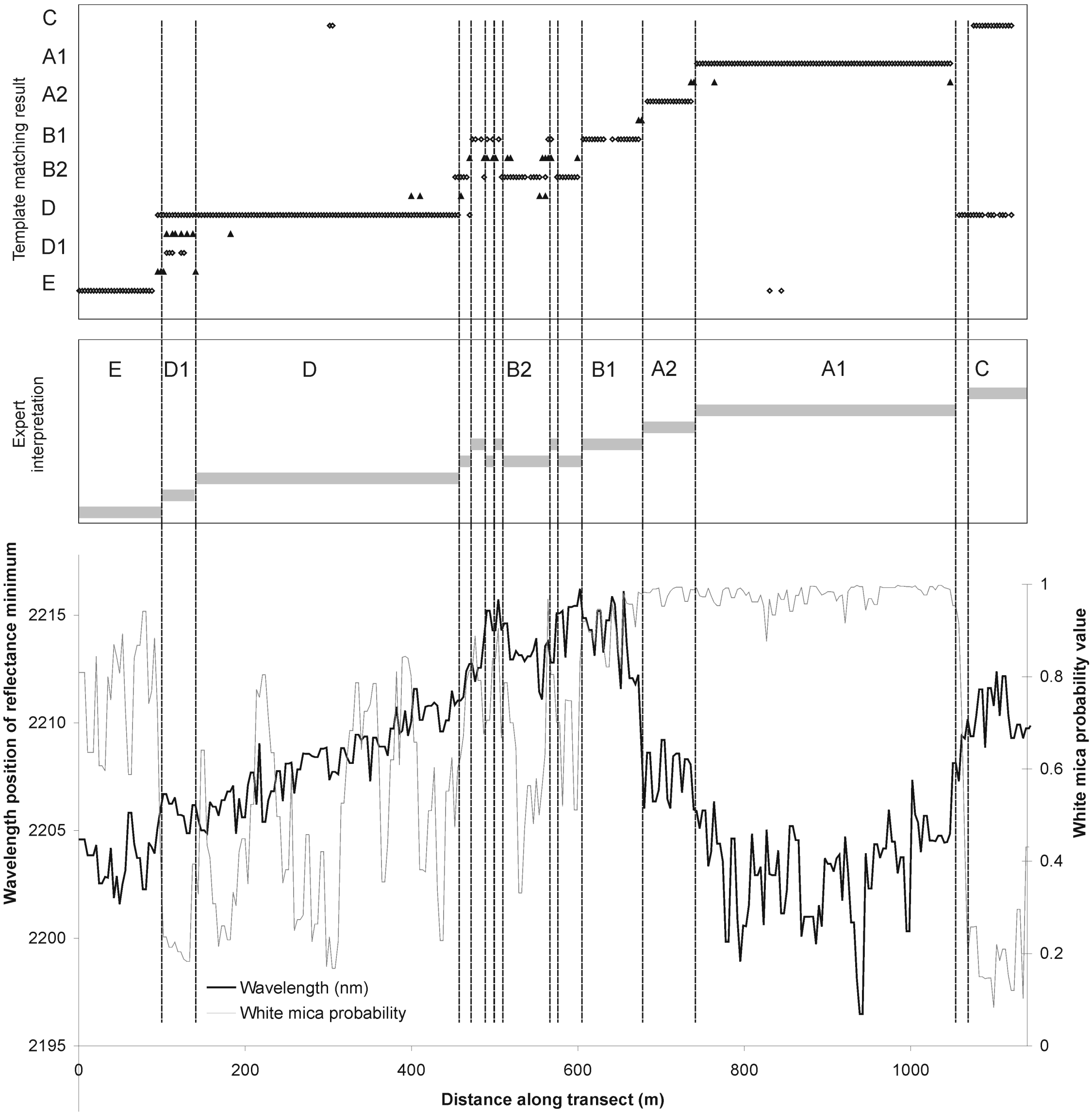

Figure 4: Image values of processed hymap imagery (bottom), expert interpretation of geologic units and boundaries (middle), and template matching result of homogenous area and boundary detection (top) along transect. Homogenous geologic units are represented by areas A – E. Boundaries between geologic units which were determined by expert opinion are represented by vertical dashed lines. Boundaries detected by template matching between various homogenous areas are indicated by triangles (top). For location of transect see Fig. 5.

4.2 Template Design

Values of images in Figs. 5C & 5D were extracted along a transect (Fig. 5A) that cross cuts the various alteration assemblages present in the area. These values were plotted in Fig. 4 and interpreted. Several geologic units were visually interpreted (Fig. 4 (middle), Table 1) including the boundaries in between. For each of the units, which are considered to be homogenous areas, minimum and maximum values were calculated. Before calculation of the statistics outlier values were removed. Based on these statistics templates were designed for 1) detection of homogenous areas and 2) detection of boundaries between some of these homogenous areas. The settings of the fifteen templates are listed in Table 1. Each homogenous area or boundary was described by two templates, one template that matched white mica probability values and a second that matched the absorption wavelengths. By designing templates based on calculating statistics it was tried to keep the procedure objective.

		White mica probability		Absorption wavelength (nm)	
Area	**Alterarion style**	Min.	Max.	Min.	Max.
C	Chert	0.08	0.30	2208.9	2212.4
A1	Al-rich white mica alt. 1	0.92	1.00	2198.1	2206.0
A2	Al-rich white mica alt. 2	0.95	0.99	2206.0	2209.2
B1	Al-poor white mica alt. 1	0.79	0.98	2211.6	2216.2
B2	Al-poor white mica alt. 2	0.47	0.79	2211.0	2215.4
D	Chlorite-quartz altered 1	0.17	0.84	2204.8	2211.6
D1	Chlorite-quartz altered 1	0.18	0.24	2204.9	2206.7
E	Altered felsic	0.59	0.94	2201.6	2205.8

Boundary	Number of pixels	Margin
A1–C	5	2
A2–A1	0	0
B1–A2	0	0
B2–B1	0	0
D –B2	0	0
D1–D	0	0
E –D1	1	1

Table 1: Template settings.

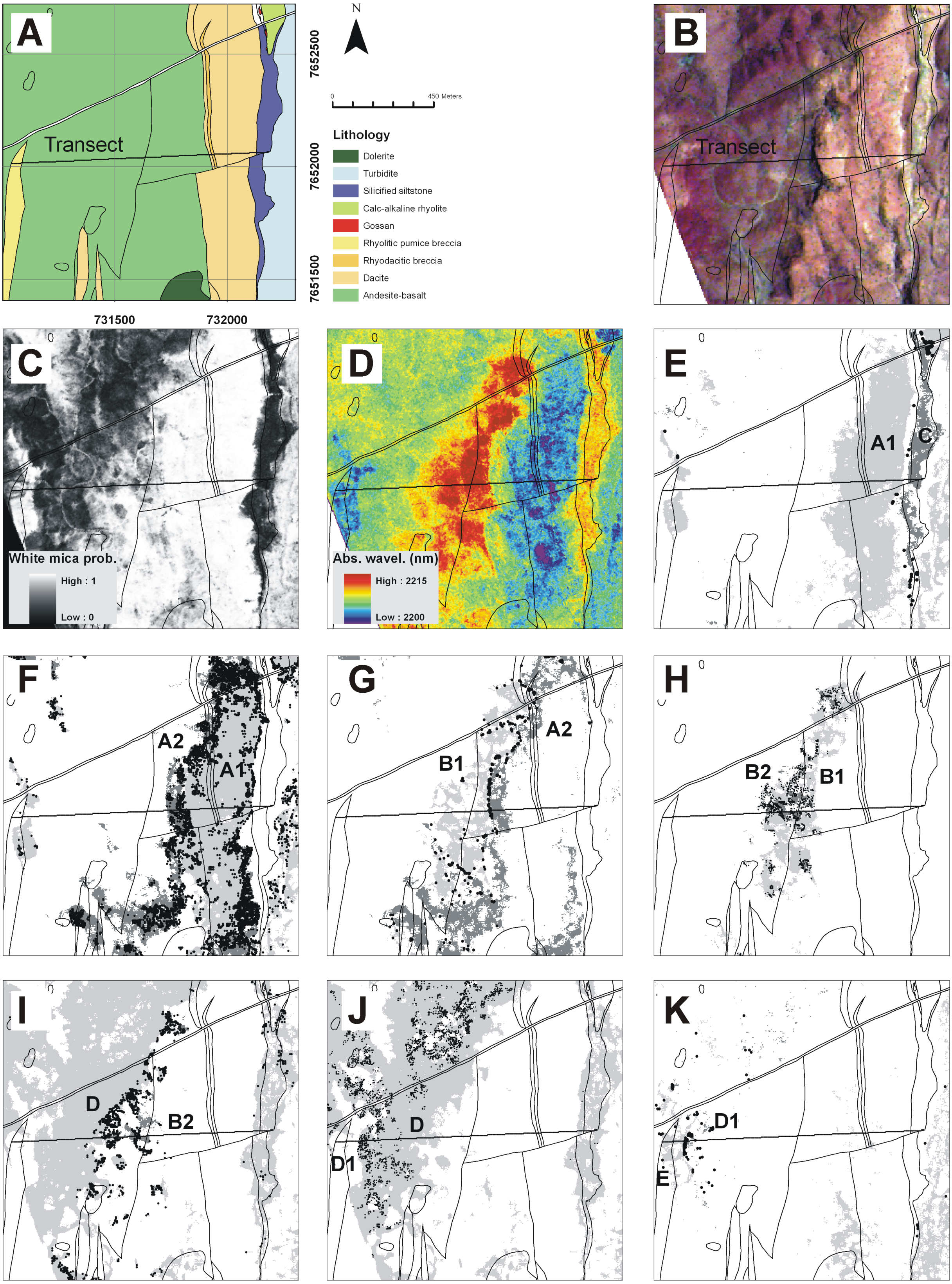

Figure 5: Lithology (after Brauhart *et al.*, 1998) of study area (A). Transect of Fig. 4 is shown in black. Processed hymap imagery, showing simulated natural colors (B), white mica probability values (C), and the wavelength position of the reflectance minimum of the main absorption feature near 2200 nm of white micas (D). Images E to K show results of template matching. In each image two homogenous areas are displayed in shades of gray and their boundary is displayed as black dots. Boundaries of geologic units from A were overlain on B – D.

5 RESULTS AND DISCUSSION

The RTM algorithm was run twice for each homogenous area and boundary. In the first run the white mica probability values were matched and in the second run the absorption wavelength values were matched using their respective templates. In an additional step the matching results of the two runs were combined. The matching results are displayed in Figs. 4 (top) and 5E – 5K. Results plotted in the transect in Figure 4 show that the matched geologic units coincide well with those interpreted by expert. Mismatches mainly occur by area D that overlaps with area D1 and C. This is not surprising since D, D1, and C are spectrally similar. Most of the boundary zones that were identified by the RTM algorithm along the transect coincide with those interpreted by expert. This results demonstrates that the method is successful, since the transect statistics were used for designing the matching templates. Only the boundary between A1 and C was not correctly identified. The reason for this is not yet clear.

Figures 5E–5K show the spatial distribution of the matching results for each combination of two neighboring geologic units and their common boundary. It shows that the continuity of the identified boundaries varies strongly between the quantified boundaries of Table 1, for instance the B1-A2 boundary in Fig. 5G is relatively continuous contrary to boundary A1-C. Also the number of matched boundaries in the area various strongly. The A2-A1 boundary is abundant while the A1-C boundary occurs sparsly. These differences in continuity and abundance are directly the result of the template design and can be changed by modifying the templates design.

The position of the boundaries that were identified by template matching reflect both changing lithology (boundaries A1-C and E-D1) and alteration conditions (boundaries A2-A1, B1-A2, B2-B1, D-B2, D1-D). The latter boundaries are the result of changes in the physico-chemical environment due the hydrothermal alteration processes. Therefore the matched boundaries provide information on geologic processes itself.

6 CONCLUSIONS

The RTM algorithm is an effective method for supervised detection of boundary zones. The characteristics of the boundary zone have to be defined in a template that is subsequently matched to an image files at various rotation angles. Application of RTM algorithm to synthetic and Hymap imagery showed that the boundary detection method is selective and only positively identifies boundaries that are quantified in the template.

Zones of changing mineralogy in the Kangaroo Caves test area reflect changing physico-chemical conditions due to hydrothermal processes. Detection of these boundary zones using airborne spectral indicator images provides information on the hydrothermal processes themselves. It is therefore concluded that the RTM algorithm provides means for processed based mapping which goes beyond mapping individual minerals or other surface materials.

References

Bakker, W and K Schmidt, 2002. Hyperspectral edge filtering for measuring homogeneity of surface cover types. *ISPRS Journal of Photogrammetry and Remote Sensing* 56(4), 246–256.

Brauhart, C, D Groves, and P Morant, 1998. Regional alteration systems associated with volcanogenic massive sulfide mineralization at Panorama, Pilbara, Western Australia. *Economic Geology* 93(3), 292–302.

Choi, M.-S and W.-Y Kim, 2002. A novel two stage template matching method for rotation and illumination invariance. *Pattern Recognition* 35, 119–129.

Cocks, T, R Jenssen, A Stewart, I Wilson, and T Shields, 1998, October). The HyMap airborne hyperspectral sensor: the system, calibration and performance. In M Schaepman, D Schläpfer, and K Itten (Eds.), *Proceedings of the 1st EARSeL workshop on Imaging Spectroscopy, 6–8 October 1998, Zürich, Switzerland*, Remote Sensing Laboratories, University of Zürich, Switzerland, pp. 37–42.

Cudahy, T, K Okada, K Ueda, C Brauhart, P Morant, D Huston, T Cocks, J Wilson, P Mason, and J Huntington, 1999. Mapping the Panorama VMS-style alteration and host rock mineralogy, Pilbara Block, using airborne hyperspectral VNIR-SWIR data. MERIWA report 205(661 R), CSIRO Exploration and Mining.

Kruse, F, A Letkoff, J Boardmann, K Heidebrecht, A Shapiro, P Barloon, and A Goetz, 1993. The spectral image processing system (SIPS) – interactive visualization and analysis of imaging spectrometer data. *Remote Sensing of Environment* 44(2–3), 145–163.

Tsai, D.-M and C.-H Chiang, 2002, January). Rotation-invariant pattern matching using wavelet decomposition. *Pattern Recognition Letters* 23(1–3), 191–201.

Tsai, D.-M and C.-H Yang, 2005, October). A quantile-quantile plot based pattern matching for defect detection. *Pattern Recognition Letters* 26(1–3), 1948–1962.

Ullah, F and S Kaneko, 2004. Using orientation codes for rotation–invariant template matching. *Pattern Recognition* 37, 201–209.

van der Werff, H, F van Ruitenbeek, M van der Meijde, F van der Meer, S de Jong, and S Kalubandara, 2005. Rotation-variant template matching for detection of complex objects. *IEEE Geoscience and Remote Sensing Letters*. accepted.

Van Ruitenbeek, F, T Cudahy, H M., and F van der Meer, 2005. Tracing fluid pathways in fossil hydrothermal systems with near-infrared spectroscopy. *Geology* 33(7), 597–600.

Van Ruitenbeek, F, P Debba, F van der Meer, T Cudahy, M van der Meijde, and M Hale, 2006. Mapping white micas and their absorption wavelengths using hyperspectral band ratios. *Remote Sensing of Environment*. in press.